The Astrophysical Journal, 896:149 (5pp), 2020 June 20 https://doi.org/10.3847/1538-4357/ab91b9

Study of the Influence of the Solar Wind Energy on the Geomagnetic Activity for Space Weather Science

Daniele Telloni[1], Francesco Carbone[2], Ester Antonucci[1], Roberto Bruno[3], Catia Grimani[4,5], Umberto Villante[6], Silvio Giordano[1], Salvatore Mancuso[1], and Luca Zangrilli[1]
[1] National Institute for Astrophysics—Astrophysical Observatory of Torino, Via Osservatorio 20, I-10025 Pino Torinese, Italy; daniele.telloni@inaf.it
[2] National Research Council—Institute of Atmospheric Pollution Research c/o University of Calabria, I-87036 Rende, Italy
[3] National Institute for Astrophysics—Institute for Space Astrophysics and Planetology, Via del Fosso del Cavaliere 100, I-00133 Roma, Italy
[4] University of Urbino Carlo Bo, Department of Pure and Applied Sciences, Via S. Chiara 27, I-61029 Urbino, Italy
[5] National Institute for Nuclear Physics, Section in Florence, Via B. Rossi 1, I-50019 Sesto Fiorentino, Italy
[6] University of L'Aquila, Department of Physical and Chemical Sciences, Via Vetoio 1, L'Aquila, Italy
Received 2020 April 13; revised 2020 May 7; accepted 2020 May 7; published 2020 June 23

Abstract

This paper addresses the investigation of the interaction of the solar wind energy with the Earth's magnetosphere, by studying its correlation with the disturbance storm time (Dst) index, a proxy of the geomagnetic activity. Some relevant parameters of the solar wind (the bulk speed and the z-component of the interplanetary magnetic field) are explored in the energy−Dst space. It results that (i) the solar wind energy and the geomagnetic activity are strictly related, with the coronal mass ejections representing the most energetic and geoeffective driver; (ii) the slow solar wind has negligible effects on Earth regardless of its energy content, whereas high-speed streams may induce severe geomagnetic storming depending on the advected energy; and (iii) while at low and mid energies, geomagnetic disturbances are induced provided the magnetic reconnection between the interplanetary and terrestrial magnetic fields occurs, high-energy solar wind plasma can impact Earth even without reconnecting with the geomagnetic field at the dayside magnetopause. The most significant result in the framework of space weather science resides in the observational evidence that the Earth's magnetosphere has a maximum response to the energetic content of the solar wind, which leads to the derivation of an empirical law allowing the proper forecast of the upper limit of the intensity of any geomagnetic disturbance on the basis of the solar wind energy derived in situ at the Lagrangian point L1.

Unified Astronomy Thesaurus concepts: Magnetohydrodynamics (1964); Heliosphere (711); Solar wind (1534); Space weather (2037); Solar-terrestrial interactions (1473)

1. Introduction

In the solar–terrestrial system, the solar wind (a continuous supersonic and super-Alfvénic flow of magnetized plasma emitted by the Sun's outer atmosphere, the corona, permeating the interplanetary space) impacts the Earth's magnetosphere, perturbing the near-Earth space environment. The study of the Sun–Earth interaction and of all the possible correlated phenomena is named space weather. A rich variety of interplanetary structures can lead to magnetospheric disturbances. Among them, coronal mass ejections (CMEs, massive bursts of high-energy plasma and magnetic field from the solar corona into the heliosphere), crossings of the heliospheric current sheet (HCS, the surface separating the two opposite magnetic polarity heliospheric hemispheres), corotating interaction regions (CIRs, compression regions generated at the interface between fast and slow flows and characterized by enhanced values of density, magnetic field, and thermal energy), and high-speed streams (HSSs), represent the main sources of the most intense events, known as geomagnetic storms. The study of the space weather phenomena has been receiving increasing attention in recent years, especially with the aim of forecasting large storm events, which are known, for example, to (i) perturb the satellites' orbits and signals, (ii) affect radio communication and navigation systems, (iii) damage power transmission grids, and (iv) pose radiation hazards to astronauts.

The solar wind controls the magnetospheric and ionospheric electric current system. In particular, during geomagnetic storms, the ring current (namely, a westward current flow around Earth due to particle drift) is strongly intensified in the Earth's magnetosphere, modifying the horizontal component of the magnetic field observed on the ground. These variations are usually quantified by the disturbance storm time (Dst) index, which is hourly derived from the measurements of four mid-latitude Earth-based geomagnetic stations. The Dst index is thus conventionally designed to estimate the ring current intensity and, in turn, to monitor the storm severity. According to Cander & Mihajlovic (1998), geomagnetic storms are thus classified as moderate, intense, or super storms, according to the value reached by the Dst index during the geomagnetic event (Dst $\in(-100, -50]$ nT, Dst $\in(-250, -100]$ nT, Dst $\in(-\infty, -250]$ nT, respectively).

Previous literature focused on the study of the influence of the dynamic pressure P of the solar wind on the Earth's magnetosphere. The geomagnetic Dst index has indeed been proved to be sensitive to P variations. Burton et al. (1975) first provided an empirical law ($\mathrm{Dst} \propto -\sqrt{P}$) relating the effects of the solar wind pressure on the Dst index. Several revisions and improvements to Burton equations were later developed by O'Brien & McPherron (2000), Wang et al. (2000), Ballatore & Gonzalez (2003), Siscoe et al. (2005), and many others.

During geomagnetic storms a huge amount of solar wind (kinetic and magnetic) energy is transferred to the Earth's magnetosphere, through magnetic reconnection at the dayside magnetopause, which takes place when the interplanetary magnetic field (IMF) is southwardly oriented (namely,

oppositely directed with respect to the geomagnetic field), allowing the solar wind to be linked the the magnetosphere. High levels of kinetic energy may lead to compression of the magnetosphere on the sunward side. On the other hand, the solar wind magnetic energy might be converted into thermal energy, heating the ionosphere and the thermosphere leading them to expand. In both cases, the release of the solar wind energy to the near-Earth space environment severely perturbs the magnetosphere–ionosphere current system, causing the geomagnetic disturbances outlined above. Therefore, the energy, rather than the dynamic pressure, of the solar wind appears to be the crucial parameter to study the relationship between the solar wind driver and the magnetospheric response, for space weather predictions. Nevertheless, little effort has been devoted until now to the investigation of the influence of the total energy carried by the solar wind on the Dst index. The reason probably lies in the difficulties associated with the local estimation of the solar wind kinetic and magnetic energies. These MHD quantities are indeed defined as

$$E_k = \frac{1}{2}\int \boldsymbol{V}^2\, d^3\boldsymbol{r} \quad \text{and} \quad E_m = \frac{1}{2}\int \boldsymbol{B}^2\, d^3\boldsymbol{r}, \tag{1}$$

where $\boldsymbol{V}(\boldsymbol{x}, t)$ and $\boldsymbol{B}(\boldsymbol{x}, t)$ are the velocity and magnetic field vectors, respectively, and the integrals are computed over the entire field-containing regions. Equation (1) implies that the evaluation of E_k and E_m depends on the knowledge of the spatial properties of the velocity and magnetic field topology, which cannot be deduced from single-spacecraft measurements only. The only way to get information on E_k and E_m even with data gathered with a single spacecraft is to redefine the kinetic and magnetic energy in the frequency domain, through their power spectra, preventing the possibility to locally estimate these quantities.

Recently, Telloni et al. (2019; Paper I, hereafter) developed a novel space weather tool, aimed at the identification of CMEs at the Lagrangian point L1 and the forecast of their geoeffectiveness. In this paper, the wavelet transforms are used to explore the kinetic and magnetic energy of the solar wind also in the time domain. Since more intense geomagnetic disturbances are expected when the energy content of the solar wind is larger (as long as the IMF remains southwardly directed), Paper I concluded by arguing that the investigation of the response of the magnetosphere to the solar wind energy content might represent a step forward in the understanding of the solar wind–magnetosphere coupling. This is the main aim of the present paper, which deals with the interaction of the solar wind with the Earth's magnetosphere on the basis of the study of the relationship between the wind energy and the Dst index. The methodological approach used to derive the energy content carried by the solar wind is described in Section 2, the results obtained from the correlation analysis between the wind energy and the Dst index are presented in Section 3, followed by a discussion in the framework of space weather predictions in Section 4.

2. Estimation of the Solar Wind Energy

The study of the influence of the solar wind energy on the geomagnetic activity is accomplished on a 12 yr time interval (from 2005 January to 2016 December), in order to increase the likelihood of statistical convergence.

In situ magnetic field and plasma measurements, acquired at a cadence of 92 s by the magnetic field investigation (Lepping et al. 1995) fluxgate magnetometer and the Solar Wind Experiment (SWE; Ogilvie et al. 1995) Faraday cup instrument on board the Wind spacecraft, orbiting around L1 upstream of the Earth, are used to derive the total (kinetic plus magnetic) solar wind energy in both the frequency and time domain. Using the Paul-wavelet transform (which has the best time resolution among the wavelet mother bases; Torrence & Compo 1998), Equation (1) can be rewritten, as a function of time t and wavenumber k, as

$$E_k(k, t) = \frac{1}{2}\sum_{i=x,y,z} \widetilde{V}_i(k, t) \text{ and } E_m(k, t) = \frac{1}{2}\sum_{i=x,y,z} \widetilde{B}_i(k, t), \tag{2}$$

where $\widetilde{V}_i(k, t)$ and $\widetilde{B}_i(k, t)$ are the wavelet transforms of the velocity and magnetic field vector components, respectively.

Since the total energy fluctuation spectrum falls with $k^{-5/3}$ (or steeper) in the solar wind, the power is dominated by the lower frequencies. Hence, in order to bring out energy structures potentially hidden by the large-scale solar wind energy, the total energy spectrogram $E(k, t) = E_k(k, t) + E_m(k, t)$ is compensated (slightly differently from Paper I) by dividing $E(k, t)$ by its global wavelet spectrum $\int E(k, t)dt$ (which can be considered a measure of the background spectrum against which local peaks can be compared; Torrence & Compo 1998). The resulting total energy spectrum $E(k, t)\Big/\int E(k, t)dt$ is thus flat and allows the identification of energy structures superposed to the solar wind energy background, regardless of the particular scale of the event. As explained in the following, the smallest and largest scales of interest in the present analysis are 1 and 73 hr. Hence, the compensated spectrum is integrated over the 1–73 hr scale range to obtain the total energy time series

$$E(t) = \int_{1\text{ hr}}^{73\text{ hr}} E(k, t)\Big/\left[\int E(k, t)dt\right] dk, \tag{3}$$

which is used to study the variability of this quantity in the solar wind at L1. It is worth noting that the total energy E as defined in Equation (3) is dimensionless.

The geomagnetic activity is instead monitored by studying the evolution of the time series of the 1 hr resolution Dst index. Since E and Dst are sampled at different time resolution, in order to perform temporal correlation analyses between the two time series, the solar wind energy E is downsampled to 1 hr (the possibility of oversampling the Dst data set has been excluded in order not to introduce artificial timescales in the geomagnetic index variations). In turn, the lower limit of the integration of $E(k, t)$ is set to 1 hr (Equation (3)).

The present study of the solar wind–magnetosphere coupling is based on the correlation analysis of the solar wind energy and Dst time series. However, these two data sets refer to two different space regions 1.5 million kilometers apart, one in the solar wind at L1, 1 hr or so (depending on the bulk speed) upstream of the magnetosphere, and the other on Earth. Hence, in order to correlate E and Dst, these time series are to be first time-shifted of their intrinsic delay τ, which includes both the transit time from L1 to Earth (say a geometrical delay) and the time required to the solar wind plasma to perturb the magnetosphere–ionosphere current system, thus inducing geomagnetic disturbances (say a physical delay). The former is relatively simple to deal with: its estimation requires

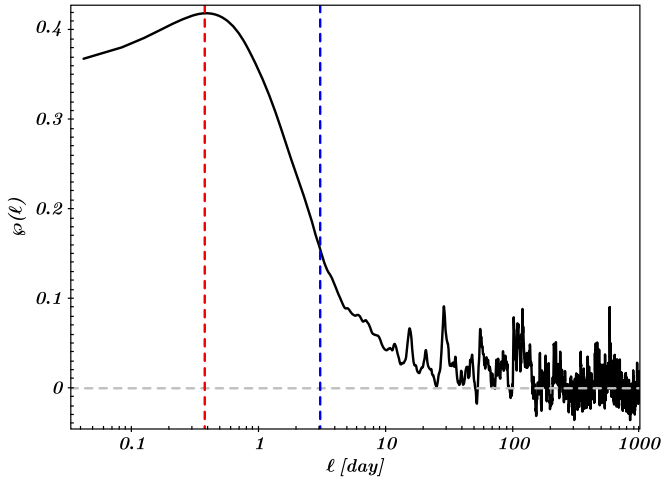

Figure 1. Cross-correlation function $\wp(\ell)$ of E and Dst as a function of the lag ℓ; red and blue dashed lines identify the time lags where $\wp(\ell)$ maximizes and assumes the $1/e$ of the peak value, respectively, namely where E and Dst are correlated at most and, conversely, where they can be considered completely uncorrelated; the horizontal gray dashed line shows, for reference, the null value.

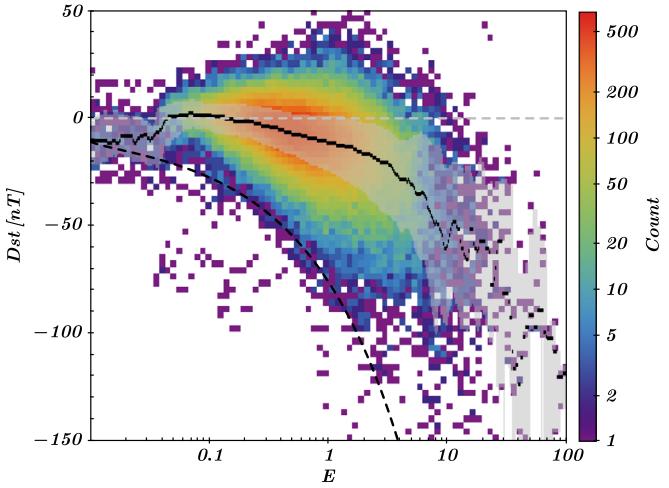

Figure 2. 2D histogram of the Dst index measurements as a function of the solar wind energy E; the black solid line represents the most likely Dst value in each energy bin, within the 68% level confidence interval (shaded gray area); the horizontal gray dashed line shows the null Dst value, corresponding to the unperturbed current system; the $E-$Dst distribution is bounded on the lower side by the dashed black line, which represents the maximum response of the magnetosphere to the energy content carried by the solar wind plasma.

information only on the bulk speed, assuming that solar wind parameter values observed at L1 by Wind at a given time will be seen at a different place at the time that the solar wind sweeps over that location. Conversely, the latter is not yet measured and is thus largely unknown. An indirect evaluation of the time delay τ was provided, though only for CMEs and not considering the different sizes of these events, in Paper I, where the waiting time between the CME detection at L1 and the onset of the induced geomagnetic effects were measured. It was found to lie, with a confidence level of 98%, in the time interval from 2 to 8 hr.

The approach adopted in this paper to infer the delay τ is based on the computation of the cross-correlation $\wp(\ell)$ of E and Dst time series as a function of the lag ℓ

$$\wp(\ell) = \frac{\sum_{i=1}^{N-\ell}(E_i - \overline{E})(\mathrm{Dst}_{i+\ell} - \overline{\mathrm{Dst}})}{\left[\sum_{i=1}^{N}(E_i - \overline{E})^2 \sum_{i=1}^{N}(\mathrm{Dst}_i - \overline{\mathrm{Dst}})^2\right]^{1/2}}, \qquad (4)$$

where $\overline{()}$ denotes the mean of the sample population and N is the number of points of the time series: the time lag where $\wp(\ell)$ maximizes will thus represent the intrinsic delay τ between the solar wind energy E and the resulting geomagnetic Dst index. Figure 1 shows the cross-correlation function $\wp(\ell)$ of E and Dst.

The $\wp(\ell)$ function peaks at $\ell = 9$ hr (red dashed line), which is thus assumed to represent the total (geometrical plus physical) delay τ between the timings of solar wind and geomagnetic correlated variations. It is not so far from the 98% 2–8 hr confidence time interval found in Paper I. The difference between the two estimates may reside in the fact that while in Paper I only CMEs were considered, $\tau = 9$ hr refers to any geoeffective solar structure, including also HSSs, CIRs, and HCS crossings (the observational evidence of a broad peak in the $\wp(\ell)$ is indicative of an average value relative to different solar wind events). While this result cannot be considered final, since this is a simplified approach neglecting any variation level in the solar wind during the solar cycle, as well as the nature of the flow (i.e., fast or slow), the adopted time-shift technique accounts for both the different locations of observation of the Wind spacecraft and the ground magnetic stations, and the finite response time of the Earth's magnetosphere to solar wind energy variations. The blue dashed line in Figure 1 indicates the time lag where $\wp(\ell)$ assumes the $1/e$ value of the maximum. This timescale, equal to 73 hr, represents the correlation length: for time lags larger than $\ell = 73$ hr the E and Dst time series can be considered completely uncorrelated. This motivates having set at 73 hr the upper limit of integration in Equation (3).

The time series of the solar wind energy is hence backward time-shifted by 9 hr (that is by nine data points) with respect to the Dst data set: $E(t) \rightarrow E(t+\tau) \doteq E(t)$. The shifted (say synchronized) E and Dst data samples can be then analyzed to study the effects of solar wind energy variations on the magnetosphere, whose results are presented in the next section.

3. Correlation between Solar Wind Energy and Dst Index

Figure 2 displays the 2D histogram of the Dst index in bins of solar wind energy; the black solid line represents the most probable value.

The $E-$Dst distribution shows how and to what extent the geomagnetic activity is regulated by the energy content of the solar wind. A general trend of enhanced perturbation of the magnetospheric current system for larger E (with Dst index lowered by 150 nT for the most energetic plasma) is indeed clearly visible. The quiet, background geomagnetic condition in the magnetosphere (Dst $\in[-10, 10]$ nT) corresponds to solar wind fluctuations with energies below $\sim$0.2. The strong evidence for a robust correlation between the amount of energy stored in the solar wind interacting with the Earth's magnetosphere and the intensity of the induced geomagnetic disturbance, as outlined by Figure 2, represents the main result of this study. The above analysis has been performed also in a three-year period centered both on the minimum (2007–2009) and the maximum (2012–2014) of the solar cycle 24, in order to test whether or not the solar cycle activity may affect the current findings. The results obtained for the solar minimum and maximum (not shown) are very similar to Figure 2, thus indicating that the different solar activity does not affect the

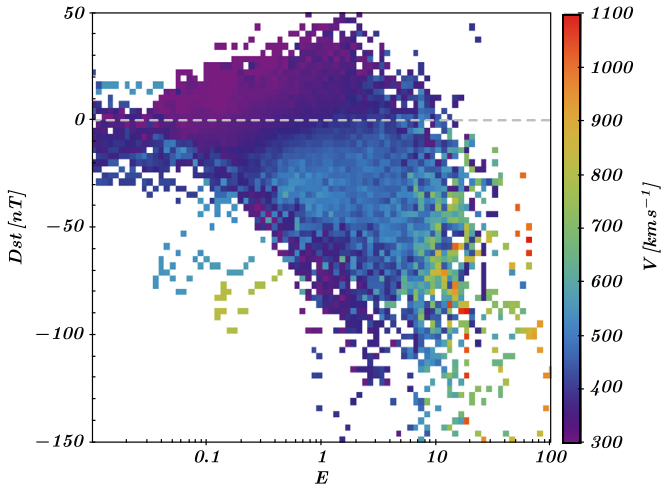

Figure 3. 2D histogram of the median value of the solar wind bulk speed V in the $E-$Dst space; the horizontal gray dashed line shows the quiet geomagnetic condition (Dst = 0) value.

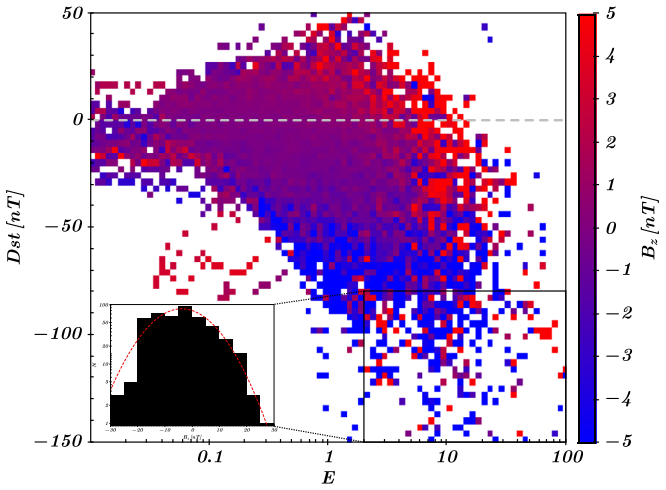

Figure 4. Same as Figure 3, but for IMF z-component B_z; the inset figure displays the B_z distribution in the region $2 < E < 100$ and $-80 <$ Dst < -150 nT (indicated by the box), superposed by a Gaussian fit (red dashed line).

strict relation existing between the solar wind energy and the geomagnetic activity, except for the fact that, as expected, during the high activity phase the solar wind is more energetic and therefore more intense geomagnetic events are driven during solar maximum than during solar minimum.

In order to recover additional information about the solar wind–magnetosphere coupling, the solar wind bulk speed V and the IMF z-component B_z are binned in the $E-$Dst space. This allows the separation of the contribution of high- and low-speed flows and the assessment of the importance of a southward orientation of the IMF in the study of the solar wind energy influence on the geomagnetic activity. Figures 3 and 4 show the median values of V and B_z, respectively, in the $E-$Dst plane.

The slow solar wind plasma ($V < 400\,\mathrm{km\,s^{-1}}$) occupies a significant extent of the parameter space, with energies spanning more than two decades ($0.01 < E < 1$) and Dst values positive or close to zero. Thus, the slow wind corresponds to a region stable with respect to magnetospheric ring currents. It is worth reminding that the intensity of ring current index Dst in quiet days is about 20 nT (Burton et al. 1975). This means that low-speed streams negligibly impact the geomagnetic field regardless of the advected energetic content. On the other hand, away from the unperturbed regions, the solar wind speed is $V \gtrsim 500/600\,\mathrm{km\,s^{-1}}$. That is, periods of mid and high geomagnetic activity correspond to HSSs. The extreme geomagnetic events (Dst < -100 nT) occur in the region of parameter space dominated by CMEs, which represent the most energetic ($E > 10$), fastest ($V \gtrsim 800\,\mathrm{km\,s^{-1}}$), and most geoeffective driver.

For what concerns the role played by the IMF orientation in the solar wind interaction with the Earth's magnetosphere, it is first necessary to point out that in order for IMF and Earth's magnetic field to reconnect, a southward orientation of the IMF is required. Therefore, the magnetic reconnection is more efficient for larger negative values of the z-component of the IMF (namely, when the orientation of the IMF is more pronounced in the southward direction). Figure 4 shows that when the solar wind is relatively less energetic ($E \lesssim 5$), the intensity of any geomagnetic disturbance (as deduced by the Dst index values) strictly depends on the value of B_z, with more and more intense geomagnetic events occurring when the negative value of B_z becomes, on average, larger and larger and, thus, the IMF is increasingly directed toward the south. In other words, as expected, at low and mid solar wind energies, the more efficient the magnetic reconnection the more intense the geomagnetic activity. While at low solar wind energies a southward direction of the IMF results to be therefore a sine qua non condition for high geomagnetic activity (as indicated by a predominance of blue bins in Figure 4 for $E \lesssim 5$ and Dst $\lesssim -75$ nT), in the high-energy and perturbed regions, B_z can also assume positive values (as evidenced by red bins in Figure 4 for $E \gtrsim 5$ and Dst $\lesssim -75$ nT). The inset plot of Figure 4 reports the distribution of the B_z values assumed in the $E-$Dst plane in the region $2 < E < 100$ and $-80 <$ Dst < -150 nT (indicated by the box). It transpires that B_z is distributed nearly randomly around the zero value, as also evidenced by the Gaussian fit (shown as a red dashed line), whose mean and deviation standard are around -3.9 nT and 10.4 nT, respectively. Thus, at high solar wind energies, there is a near equipartition between positive and negative values of B_z. It turns out that if the solar wind energy is sufficiently high, intense geomagnetic activity (with a Dst < -80 nT) are not necessarily associated with southward directions of the IMF, which therefore do not result in being crucial in driving geomagnetic disturbances (in fact, if a southward direction of the IMF were the only crucial parameter for the onset of geomagnetic disturbances, the $E-$Dst distribution displayed in Figure 2 should moreover be isotropically distributed and should not exhibit a clear trend that correlates E and Dst values, as instead observed). It can be thus concluded that when high-energy flows ($E \gtrsim 5$) arrive at Earth, geomagnetic events can be triggered even with a northward direction of the IMF, namely without magnetic reconnection between the interplanetary and terrestrial magnetic fields. As a matter of fact, either the compression or the expansion of the magnetosphere drives the intensification of ring currents regardless of the particular IMF orientation. Plasma flows carrying a large amount of kinetic energy can significantly compress the magnetosphere. Similarly, since magnetic energy is converted into thermal energy during the interaction with the geomagnetic field, the magnetosphere is heated (and, in turn, expanded) when highly magnetized solar wind streams impact on Earth. Therefore, high-energy solar events can severely perturb the near-Earth space environment independently of the IMF direction. This result provides evidence

that the crucial parameter in the Sun–Earth interaction is the energy carried by the solar wind.

The result that magnetic reconnection may not be crucial in driving intense geomagnetic disturbances has already been observed and reported in the literature by Hasegawa et al. (2004a, 2004b). On the basis of a statistical study of *Geotail* data, Hasegawa et al. (2004b) noted that the plasma in low-latitude boundary regions of the Earth's magnetosphere is denser during northward IMF periods (contrarily to what is expected if the magnetic reconnection were the dominant process), arguing that significant heating, due to the solar wind, could occur at the flanks of the Earth's magnetic field. Later on, Hasegawa et al. (2004a) showed that under northward IMF, and thus even without the presence of magnetic reconnection, the solar wind enters the Earth's magnetosphere, driving various space weather phenomena, via a mechanism associated with the nonlinear phase of the Kelvin–Helmholtz instability.

4. Space Weather Science Implications

Any space weather study aimed at forecasting geomagnetic events should predict, in addition to the arrival time at Earth of potentially geoeffective solar structures, (i) the likelihood of their geoeffectiveness and (ii) the intensity of the likely induced geomagnetic disturbance. In this context, the present analysis represents a step forward in space weather science, since it allows the forecast of the most probable geomagnetic activity and of the interval (with the desired level of confidence) of the corresponding induced Dst index variations, once the solar wind energy is derived at L1 on the basis of the method described above. From the $E-$Dst distribution displayed in Figure 2, it is possible to estimate the most likely Dst value in each energy bin (black solid line) within the 68% level confidence interval (shaded gray area), regardless of the solar event type impacting on Earth and of the physical processes underlying the solar wind–magnetosphere interaction. As an example, if the energy measured in the solar wind at L1 were 1, an enhancement of the geomagnetic activity would be registered as a decrease of the Dst index at values lying, with a confidence level of 68%, between −25 and 0 nT. The alert will be provided 9 hr in advance (the mean time delay between E and Dst data, as discussed in Section 2) with respect to the onset of the geomagnetic perturbation.

More interestingly, as clearly shown by Figure 2, the Dst index appears bounded at lower values. This means that there exists a maximum response of the Earth's magnetosphere to any geoeffective solar driver, which can be inferred in terms of the energy content embedded in solar wind fluctuations. The lower Dst threshold can be fitted by an analytic function

$$\mathrm{Dst} = -10 + \frac{a}{(E - E_0)^b}, \tag{5}$$

which gives the maximum magnitude of the Dst response as a function of the solar wind energy (a, b, and E_0 are the fitted parameters). A Levenberg−Marquardt least-squares minimization gives as best values for the parameters $a = -66.58$ nT, $b = -0.55$, and $E_0 = 9.55 \times 10^{-3}$. The $E-$Dst relation obtained by substituting this set of parameters in Equation (5) (shown in Figure 2 as a dashed black line) allows the forecast of the upper limit of the intensity of the geomagnetic activity if energy E is measured in the solar wind at L1. With reference to the above example, for solar wind energy $E = 1$, the induced geomagnetic perturbations could lower the Dst index at most to a value of ~ -75 nT. The evidence of the lower boundary limit of the Dst index due to the maximum magnetospheric response offers also the important opportunity to claim when no space weather alert should be issued. Indeed, if $E \lesssim 0.4$ it can be confidently assessed that the Dst will remain above −50 nT and thus that no geomagnetic disturbances will occur.

The approach employed in this paper for the analysis of solar wind observations at 1 au can be applied to Parker Solar Probe and Solar Orbiter data to trace the evolution of the energy carried by solar wind during its expansion from the extended corona out to the inner heliosphere, thus contributing to the development of a more refined space weather tool based on plasma flow energy as a useful indicator of the level of interaction of the solar wind with Earth.

D.T. was partially supported by the Italian Space Agency (ASI) under contract I/013/12/0. Wind data and the geomagnetic Dst index were downloaded from the NASA-CDAWeb[7] and WDC-Kyoto[8] websites, respectively. D.T. wishes to thank his father Adriano Telloni for his support and encouragement whenever it was needed.

ORCID iDs

Daniele Telloni https://orcid.org/0000-0002-6710-8142
Francesco Carbone https://orcid.org/0000-0002-3559-5273
Ester Antonucci https://orcid.org/0000-0003-4155-6542
Roberto Bruno https://orcid.org/0000-0002-2152-0115
Catia Grimani https://orcid.org/0000-0002-5467-6386
Umberto Villante https://orcid.org/0000-0002-3630-7958
Silvio Giordano https://orcid.org/0000-0002-3468-8566
Salvatore Mancuso https://orcid.org/0000-0002-9874-2234
Luca Zangrilli https://orcid.org/0000-0002-4184-2031

References

Ballatore, P., & Gonzalez, W. D. 2003, EP&S, 55, 427
Burton, R. K., McPherron, R. L., & Russell, C. T. 1975, JGR, 80, 4204
Cander, L. R., & Mihajlovic, S. J. 1998, JGR, 103, 391
Hasegawa, H., Fujimoto, M., Phan, T.-D., et al. 2004a, Natur, 430, 755
Hasegawa, H., Fujimoto, M., Saito, Y., & Mukai, T. 2004b, GeoRL, 31, L06802
Lepping, R. P., Acũna, M. H., Burlaga, L. F., et al. 1995, SSRv, 71, 207
O'Brien, T. P., & McPherron, R. L. 2000, JGR, 105, 7707
Ogilvie, K., Chornay, D., Fritzenreiter, R., et al. 1995, SSRv, 71, 55
Siscoe, G. L., McPherron, R. L., & Jordanova, V. K. 2005, JGR, 110, A12227
Telloni, D., Antonucci, E., Bemporad, A., et al. 2019, ApJ, 885, 120
Torrence, C., & Compo, G. P. 1998, BAMS, 79, 61
Wang, C. B., Chao, J. K., & Lin, C. H. 2000, JGRA, 108, 1341

[7] https://cdaweb.sci.gsfc.nasa.gov/index.html
[8] http://wdc.kugi.kyoto-u.ac.jp/index.html